

See discussions, stats, and author profiles for this publication at: <https://www.researchgate.net/publication/282438397>

First-Principles Prediction of the Charge Mobility in Black Phosphorus Semiconductor Nanoribbons

ARTICLE in JOURNAL OF PHYSICAL CHEMISTRY LETTERS · OCTOBER 2015

Impact Factor: 7.46 · DOI: 10.1021/acs.jpclett.5b01644

READS

15

6 AUTHORS, INCLUDING:



Jin Xiao

Central South University

23 PUBLICATIONS 458 CITATIONS

[SEE PROFILE](#)



Hui Xu

Central South University

43 PUBLICATIONS 131 CITATIONS

[SEE PROFILE](#)



Kwok sum Chan

City University of Hong Kong

156 PUBLICATIONS 1,195 CITATIONS

[SEE PROFILE](#)

First-Principles Prediction of the Charge Mobility in Black Phosphorus Semiconductor Nanoribbons

Jin Xiao,^{†,§} Mengqiu Long,^{*,†,‡} Xiaojiao Zhang,^{||} Dan Zhang,[†] Hui Xu,[†] and Kwok Sum Chan^{*,†,‡}

[†]Institute of Super-Microstructure and Ultrafast Process in Advanced Materials, School of Physics and Electronics, Central South University, Changsha 410083, China

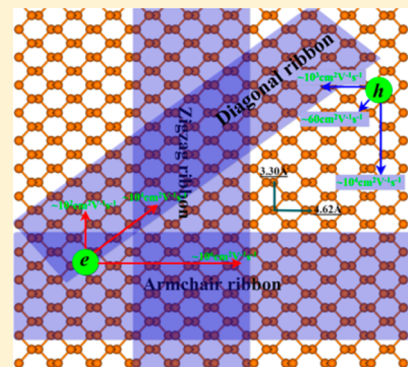
[‡]Department of Physics and Materials Science, City University of Hong Kong, Hong Kong, China

[§]School of Science, Hunan University of Technology, Zhuzhou 412007, China

^{||}Physical Science and Technology College of Yichun University, 576 Xuefu Road, Yuanzhou, Yichun 336000, China

Supporting Information

ABSTRACT: We have investigated the electronic structure and carrier mobility of monolayer black phosphorus nanoribbons (BPNRs) using density functional theory combined with Boltzmann transport method with relaxation time approximation. It is shown that the calculated ultrahigh electron mobility can even reach the order of 10^3 to $10^7 \text{ cm}^2 \text{ V}^{-1} \text{ s}^{-1}$ at room temperature. Owing to the electron mobility being higher than the hole mobility, armchair and diagonal BPNRs behave like n-type semiconductors. Comparing with the bare BPNRs, the difference between the hole and electronic mobilities can be enhanced in ribbons with the edges terminated by H atoms. Moreover, because the hole mobility is about two orders of magnitude larger than the electron mobility, zigzag BPNRs with H termination behave like p-type semiconductors. Our results indicate that BPNRs can be considered as a new kind of nanomaterial for applications in optoelectronics, nanoelectronic devices owing to the intrinsic band gap and ultrahigh charge mobility.



Owing to their unique physical properties and potential applications in nanoscale devices, 2D atomically thick materials, such as graphene,¹ graphdiyne sheet,² boron nitride sheets,³ silicene,⁴ and layered transition-metal dichalcogenides^{5–7} have attracted intensive attention. Recently, after the successful synthesis of few-layer black phosphorus (BP),^{8–11} which is called phosphorene, the 2D phosphorus materials have become the research focus of the science community.^{12–24} The bulk form of BP, which is the most stable phosphorus allotrope under normal conditions, has a direct band gap of $\sim 0.3 \text{ eV}$.^{25–27} The direct band gap will be increased to $\sim 2.0 \text{ eV}$ ^{28,29} when the BP is reduced to monolayer, which opens doors for applications in optoelectronics. Furthermore, the bulk form of BP is found to have high carrier mobility on the order of $10^5 \text{ cm}^2 \text{ V}^{-1} \text{ s}^{-1}$ at low temperatures.^{30,31} The field-effect carrier mobilities of few layers BP are found to be $\sim 1000 \text{ cm}^2 \text{ V}^{-1} \text{ s}^{-1}$ for electron⁸ and $286 \text{ cm}^2 \text{ V}^{-1} \text{ s}^{-1}$ for hole⁹ at room temperature. Also, few-layer BP exhibits ambipolar behavior with drain current modulation up to 10^5 .⁸ Owing to the direct gap and high mobilities, there is a potential for the thin BP crystals being used as a new 2D material for applications in optoelectronics, nanoelectronic devices, and so on.^{32–38}

By confining 2D bulk materials, quasi-1D materials can be created with different properties. In other atomically thick ribbon materials such as graphene and molybdenum disulfide (MoS_2), the electronic properties of the nanoribbons are mainly determined by the ribbon's edges^{39–42} as well as modified by the edge termination.⁴³ It has been found that the

carrier mobility of quasi 1D graphene ribbons is significantly lower than that of the graphene sheet owing to the removal of the massless Dirac Fermion characteristic,^{39,40} and the carrier mobility of MoS_2 nanoribbons can be regulated by edge chemical modification through the changes in the electronic structure.⁴³ Nevertheless, in BP nanoribbons (BPNRs), the states near the Fermi level are determined by the central atoms of the ribbons rather than the edge ones.^{18,24} Thus, the BPNRs would have been much more interesting with respect to the charge-transport properties; however, so far, there are very few systematic reports about the mobilities of BPNRs. In this study, by using first-principles calculations and the deformation potential theory, we systematically investigate the intrinsic mobility of BPNRs due to the acoustic phonon scattering mechanism.

The atomic structure of the BP sheet is shown in Figure 1a. The relaxed lattice constants of BP sheet in our calculation are $a_1 = 4.62 \text{ \AA}$, $a_2 = 3.30 \text{ \AA}$, in good agreement with other theoretical calculations.¹³ Along its two lattice vectors, we define two kinds of ribbon edges: armchair (edges are in parallel with \vec{a}_1) and zigzag (edges are in parallel with \vec{a}_2). The BPNRs can be classified as armchair (ABPNRs) and zigzag nanoribbons (ZBPNRs). Similar to graphene ribbons, many

Received: July 30, 2015

Accepted: October 1, 2015

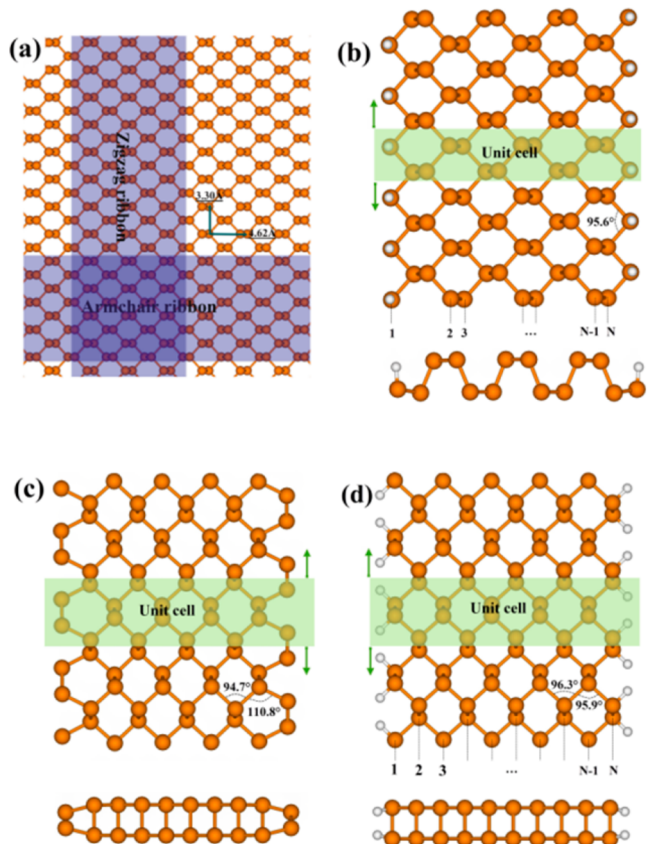


Figure 1. Models of BPNRs: (a) BP sheet, (b) H-terminated ZBPNRs, (c) bare, and (d) H-terminated ABPNRs.

chemical groups (such as CH_3 , NH_2 , and F) have been used to passivate the edge, thus leading to the promising electronic and magnetic properties. The edge modification by CH_3 and NH_2 can also be found in other graphene-based systems, such as hybrid fluorographene–graphene nanoribbons.⁴⁴ To simplify models, we choose H atoms to passivate edges. Previous studies indicate that the bare ZBPNRs are conductors,²⁴ but the energy gap of ZBPNRs will be opened when edges are terminated by H atom.³² Owing to the deformation, the potential theory method is more appropriate for semiconducting systems,⁴⁵ and the bare ZBPNRs are not considered in our study. The optimized structure of ZBPNRs with H-termination is shown in Figure 1b. In the following, ZBPNRs means H-terminated ZBPNRs. The ABPNRs are semiconductors with or without edge termination. In this paper, the bare and H-terminated ABPNRs are investigated. After atomic relaxation, the optimized structures are shown in Figure 1c,d. We use the number of saw-like lines across the ribbon width (N) to describe the different width of the ribbons (the armchair and zigzag ribbons are thus denoted by ABPNR- N and ZBPNR- N , respectively), as shown in Figure 1b,d. The black phosphorus is a puckered honeycomb structure; the 3D structures of the H-terminated ZBPNR-7 and ABPNR-11 are present by a front top view, as shown in Figure S1 in the Supporting Information (SI). From the bond angles, it can be found that the atomic structures of the BPNRs with H-termination are very close to the structure of the BP sheet, and there is edge deformation in bare ABPNRs, and the change of the atomic structure is mainly reflected in lattice length. The lattice length of ZBPNRs with H-termination is a constant ($\sim 3.30 \text{ \AA}$), which is equal to lattice

length of the BP sheet along the same direction, and the lattice length of ABPNRs as a function of N is shown in Figure S2. It can be found that the lattice length of bare ABPNRs decreases with N increasing and tends to close to 4.62 \AA , which is the lattice length of the bulk sheet. On the contrary, the lattice length of H-terminated ribbons is a constant of $\sim 4.61 \text{ \AA}$.

The energy band spectra of BPNRs are shown in Figure 2a. Here we choose bare ABPNR-10, H-terminated ABPNR-10, and H-terminated ZBPNR-7 as examples. It can be noted that H-terminated ABPNRs are direct gap semiconductors and the others (bare ABPNRs and H-terminated ZBPNRs) are indirect gap semiconductors. In bare ABPNRs, the conduction band minimum (CBM) locates at $1/3\pi$ in the wave-vector space. In H-terminated ZBPNRs, the valence band maximum (VBM) locates at $1/5\pi$ in the wave-vector space, which is $\sim 12.71 \text{ meV}$ higher than that at the Γ -point for $N = 7$, which is consistent with the previous work,¹⁸ and VBM of H-terminated ZBPNR tends to close to the Γ -point with N increasing. When $N = 12$, the VBM locates at 0.12π in the wave-vector space and the value of the gap with the Γ -point is reduced to 4.71 meV . The energy band gaps of BPNRs as a monotonic decreasing function of N are shown in Figure 2b. The band gap of H-terminated ABPNRs is larger than that of the BP sheet (0.90 eV for PBE calculation²³), decreases from 1.06 to 0.94 eV with N , and increases from 8 to 15 . There is a smaller gap when the edges are bare in ABPNRs with the same width. The band gap of $N = 8$ in ABPNRs is only 0.71 eV . The band gap of H-terminated ZBPNRs drops from 1.81 into 1.21 eV with N increases from 6 to 12 .

In the 1D case, the stretching modulus is defined as $C^{1D} = [\partial^2 E / \partial \delta^2]/L_0$, where the uniaxial strain δ is applied along the ribbon direction, L_0 is the lattice constant of the optimized ribbon, and E is the total energy of a ribbon cell. The C^{1D} of BPNRs is shown in Figure S3a,b. The deformation potential constant (E_1) is calculated as $dE_{\text{edge}}/d\delta$, where the E_{edge} denotes the energy of the conduction or valence band edge. The E_1 in BPNRs is shown in Figure S3c,d. On the basis of the obtained energy band spectrum, the values of E_1 and C^{1D} and the acoustic-phonon-limited charge mobility (μ) at room temperature (300 K) can be obtained using formulas (1) and (2) in the SI.

The room-temperature μ for the ribbons is shown in Figure 2c,d, and the μ of the 2D sheet, represented by the horizontal dot lines, is also plotted for comparison. It is clearly seen that the electron mobility (μ_e) is much higher than the hole mobility (μ_h) in ABPNRs due to the smaller electron $|E_1|$, which means that ABPNRs behave like *n*-type semiconductors for both bare and H-terminated in ambipolar transport, and we also find the mobility is significantly enhanced by edge termination. The μ_h in both bare and H-terminated ABPNRs, which is higher than the mobility of 2D sheet ($\sim 200 \text{ cm}^2 \text{ V}^{-1} \text{ s}^{-1}$ ⁴⁶), increases continuously with N . For a specific N , the μ_h in H-terminated ABPNRs is $\sim 150 \text{ cm}^2 \text{ V}^{-1} \text{ s}^{-1}$ higher than that of the bare ABPNRs. The μ_e of bare ABPNRs is oscillating around $750 \text{ cm}^2 \text{ V}^{-1} \text{ s}^{-1}$, and the highest mobility in our calculation is up to $3.46 \times 10^3 \text{ cm}^2 \text{ V}^{-1} \text{ s}^{-1}$ with $N = 9$, which is still smaller than the μ_e of sheet ($\sim 10^4 \text{ cm}^2 \text{ V}^{-1} \text{ s}^{-1}$ ⁴⁶). The μ_e of H-terminated ABPNRs, which first increases and then decreases with the increasing of N , is much higher than the μ_e of sheet, and the highest value is even up to $1.02 \times 10^7 \text{ cm}^2 \text{ V}^{-1} \text{ s}^{-1}$ with $N = 11$, which surpasses graphene ($\sim 3.39 \times 10^5 \text{ cm}^2 \text{ V}^{-1} \text{ s}^{-1}$ ⁴⁵); the lowest one is also up to $3.71 \times 10^4 \text{ cm}^2 \text{ V}^{-1} \text{ s}^{-1}$ with $N = 8$. Instead, there are higher μ_h than μ_e in ZBPNRs with H-

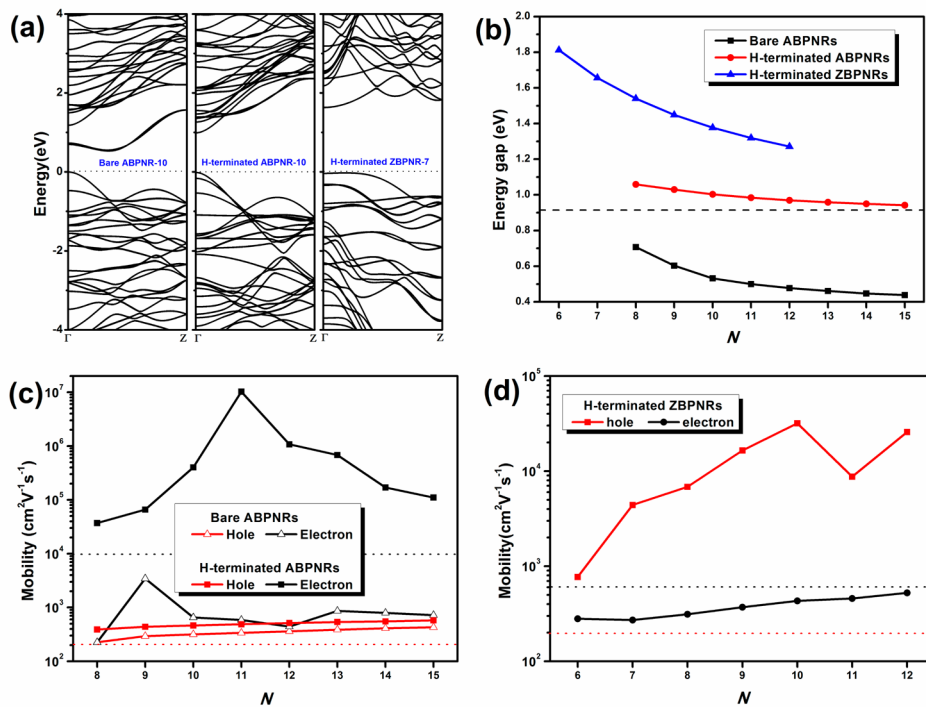


Figure 2. (a) Energy band structures of ABPNR-10 and ZBPNR-7. (b) Energy gaps as a function of N , in which the dashed line is the energy gap of monolayer BP-based on PBE calculation (0.9 eV²³). (c) Room-temperature charge mobility of ABPNRs. The red (black) dotted line is the room-temperature hole (electron) mobility in monolayer BP along the armchair direction. (d) Room-temperature charge mobility of ZBPNRs. The red (black) dot line is the room-temperature hole (electron) mobility in monolayer BP along the zigzag direction. The data of monolayer BP charge mobility are from ref 45.

termination owing to the smaller hole $|E_1|$. The μ_e (μ_h) of H-terminated ZBPNRs increases from 2.80×10^2 (7.72×10^2) to 5.24×10^2 (2.58×10^4) $\text{cm}^2 \text{V}^{-1} \text{s}^{-1}$ with $6 \leq N \leq 12$. The μ_e of H-terminated ZBPNRs is smaller than μ_e of 2D sheet along the zigzag direction ($\sim 600 \text{ cm}^2 \text{ V}^{-1} \text{s}^{-1}$ ⁴⁶), but the μ_h of H-terminated ZBPNRs is much higher than that of sheet ($\sim 150 \text{ cm}^2 \text{ V}^{-1} \text{s}^{-1}$ ⁴⁶).

On the basis of formulas (1) and (2) in the SI, there is $\mu \propto C^{1D}/E_1^2$. For bare ABPNRs (H-terminated ABPNRs), the energy band structures are very similar for difference N , so the charge mobility is decided by the value of C^{1D}/E_1^2 . For electron in bare ABPNRs, there is the biggest value of C^{1D}/E_1^2 with $N = 9$, which is $8.19 \times 10^{30} \text{ m}^{-1} \text{ J}^{-1}$, as shown in Table S1. So the bare ABPNR-9 presents higher electron mobility than other bare ABPNRs. For electron E_1 , as shown in Figure S3c,d, it can be found that the bare ABPNR-9 has the smallest value of electron $|E_1|$ (only 0.31 eV) in bare ABPNRs with $8 \leq N \leq 15$, and the H-terminated ABPNR-11 has the smallest value of electron $|E_1|$ (only 0.02 eV) in the H-terminated ABPNRs with $8 \leq N \leq 15$. The value of electron $|E_1|$ is the index of electroacoustic coupling. That means electron–phonon coupling in the bare ABPNR-9 is weaker than other bare ABPNRs. It is the same for H-terminated ABPNRs: When $N = 11$, there is the weakest electron–phonon coupling one in H-terminated ABPNRs. Because the value of C^{1D}/E_1^2 for hole in the H-terminated ZBPNR-11 ($185.98 \times 10^{30} \text{ m}^{-1} \text{ J}^{-1}$) is smaller than the ZBPNR-10 ($705.18 \times 10^{30} \text{ m}^{-1} \text{ J}^{-1}$) and ZBPNR-12

($532.08 \times 10^{30} \text{ m}^{-1} \text{ J}^{-1}$), the hole mobility in the ZBPNR-11 is smaller than that in the ZBPNR-10 and ZBPNR-12.

The band decomposed charge density around the Fermi level of BPNRs is shown in Figure 3. For bare ABPNRs, the VBM extends across the whole ribbon and has the majority in the central region of the ribbon. The contrary is the case of CBM that has the majority in the edge of the ribbon. For H-terminated ABPNRs and ZBPNRs, both the VBM and CBM are localized in the central region of the ribbons. In ABPNRs, the tensile strain applied in the ribbon direction effectively flattens the pucker of phosphorus by changing the dihedral angles (>80% of the total deformation is caused by the dihedral angles change), which can significantly reduce the required strain energy. Owing to the angle change, the P–P bond length is not significantly changed by the applied strain.³³ So the C^{1D} of ABPNRs is much smaller than that of ZBPNRs. The CBM states of H-terminated ABPNRs are only localized on the two sublayers of P atoms and they are parallel to the ribbon plane. Along the direction normal to the ribbon, there are nonbonding states to respond to the tensile strain applied. For these nonbonding states, the wave function overlap is minimal and their energies are expected to be insensitive to strain.²⁰ As a result, the E_1 of CBM in H-terminated ABPNRs is close to zero and the small E_1 causes super high mobility. It is noted that the computational error of E_1 can be very high, which results in exponential growth errors in the mobility calculation. For the case of H-terminated ABPNR-11, the electron $|E_1|$ is only 0.02 eV. In our calculation, five structural deformation models ($\delta = \pm 1, 0, \pm 0.5\%$) are used to fitting the E_1 . The difference value of the adjacent fitting data is $\sim 10^{-4}$ eV. Actually in our density function theory calculation, the precision of eigenvalue

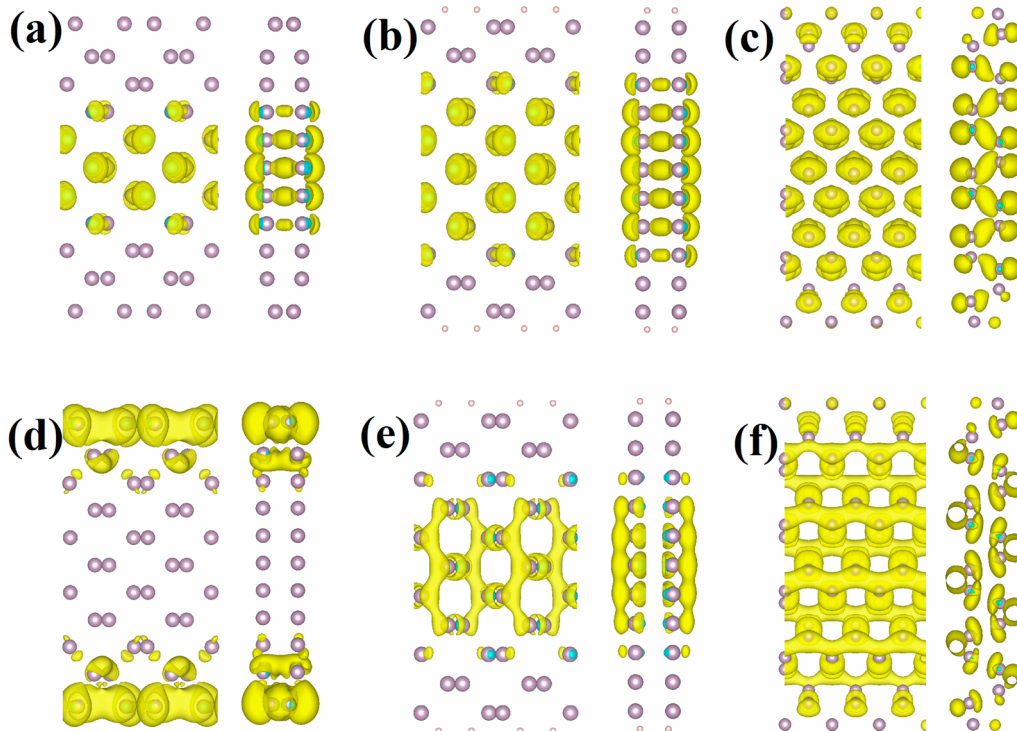


Figure 3. Band decomposed charge density of BPNRs: (a–c) Valence band edge for bare ABPNR-11, H-terminated ABPNR-11, and H-terminated ZBPNR-10, respectively. (d–f) Conduction band edge for bare ABPNR-11, H-terminated ABPNR-11, and H-terminated ZBPNR-10, respectively. Isosurface values is 3×10^{-4} e/bohr³.

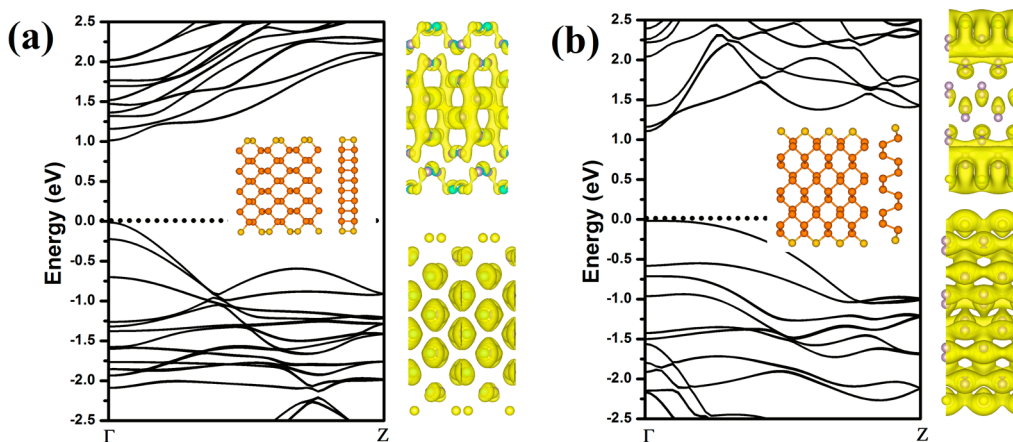


Figure 4. Energy bands of BPNRs with S atom termination: (a) ABPNR-10 and (b) ZBPNR-7.

calculation is hard to reach that high value. So the error value of electron $|E_1|$ in H-terminated ABPNR-11 will be over 100%, but even if we set the electron $|E_1|$ to twice of the old value, the electron mobility is still over 10^6 cm² V⁻¹ s⁻¹. For the hole $|E_1|$ in H-terminated ABPNR-11, which is ~3.35 eV, the difference of the adjacent fitting datas is ~0.02 eV. The precision of eigenvalue calculation is higher than that value. So the error of hole $|E_1|$ is smaller than 10%. The error of hole mobility calculation is limited under this situation. In our calculation, when the value of $|E_1|$ is more close to zero, the $|E_1|$ and mobility are more imprecise; however, it can be sure that there is considerable electron mobility in H-terminated ABPNRs based on acoustical phonon scattering. Actually, such high

mobility may not be realized in experiment, owing to the inevitable impurities and defects in the material, and they have great effects on the charge transport properties, especially at low temperature when the phonon effects are important.⁴⁵

Atomic orbital analysis shows that both the VBM and CBM are mainly composed of the out-of-plane p_z orbitals. The valence band of ABPNRs is the hybridization of ~90% of out-of-plane p_z orbitals and ~10% of s orbitals. For the conduction band of ABPNRs, the proportion of the p_x orbitals is up to ~21% for the H-terminated ABPNR-11 and ~10% for the bare ABPNR-11. It indicates that the electron can move much faster. So, the μ_e is over 1.02×10^7 cm² V⁻¹ s⁻¹ for H-terminated ABPNR-11 and over 5.87×10^2 cm² V⁻¹ s⁻¹ for bare ABPNR-

Table 1. Lattice Length (L), Energy Gap (E_{gap}), Line Stiffness (C^{1D}), Deformation Potential Constant (E_1), Electron Relaxation Time (τ_e), Hole Relaxation Time (τ_h), Electron Mobility (μ_e), and Hole Mobility (μ_h) of Phosphorous Ribbons^a

N	L (Å)	E_{gap} (eV)	C^{1D} (10^{-9} J m^{-1})	E_1 of electron (eV)	E_1 of hole (eV)	τ_e (ps)	τ_h (ps)	μ_e ($\text{cm}^2/(\text{V s})$)	μ_h ($\text{cm}^2/(\text{V s})$)
ABPNR-10	4.67	0.53	23.00	-0.77	-2.80	0.09	0.02	6.53×10^2	3.17×10^2
ABPNR-10-S	4.62	1.03	33.29	-0.44	-3.45	1.13	0.01	1.80×10^4	4.06×10^2
ABPNR-10-H	4.61	1.00	31.63	0.10	-3.22	20.93	0.02	4.01×10^5	4.63×10^2
ZBPNR-7-S	3.26	1.12	147.85	-14.20	-0.45	0.01	0.88	1.12×10^2	1.63×10^3
ZBPNR-7-H	3.30	1.66	153.75	1.93	-0.23	0.10	2.34	2.72×10^2	4.40×10^3

^aTemperature is 300 K. -S and -H represent S-atom and H-atom terminations, respectively.

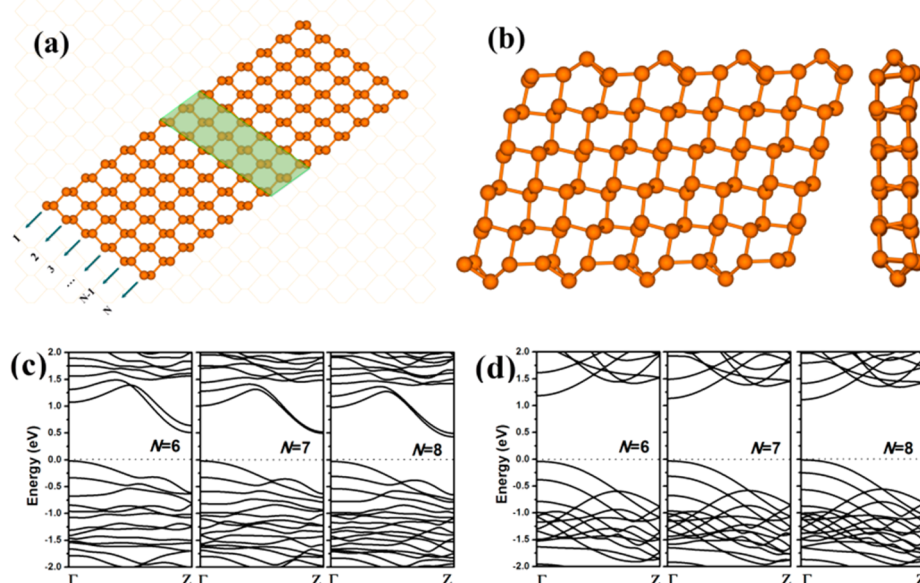


Figure 5. Model and electronic structures of DBPNRs. Atomic structures of DBPNRs (a), the optimum structure of bare DBPNRs-6 (b), and the energy band spectrum of DBPNRs: (c) bare and (d) H-terminated.

Table 2. Lattice Length (L), Energy Gap (E_{gap}), Line Stiffness (C^{1D}), Deformation Potential Constant (E_1), Electron Relaxation Time (τ_e), Hole Relaxation Time (τ_h), Electron Mobility (μ_e), and Hole Mobility (μ_h) of DBPNRs^a

N	L (Å)	E_{gap} (eV)	C^{1D} (10^{-9} J m^{-1})	E_1 of electron (eV)	E_1 of hole (eV)	τ_e (ps)	τ_h (ps)	μ_e ($\text{cm}^2/(\text{V s})$)	μ_h ($\text{cm}^2/(\text{V s})$)
6	5.49	0.53	68.09	-6.02	-3.59	0.01	0.02	1.33×10^2	53.12
7	5.51	0.52	77.70	-6.11	-3.85	0.01	0.02	1.56×10^2	52.42
8	5.53	0.46	87.50	-6.23	-4.34	0.01	0.01	1.62×10^2	45.95
6-H	5.69	1.23	58.85	0.77	-3.08	0.37	0.02	2.23×10^3	66.74
7-H	5.69	1.17	68.16	0.59	-3.25	0.73	0.02	4.40×10^3	64.46
8-H	5.69	1.13	77.98	0.33	-3.57	2.78	0.02	1.70×10^4	57.90
6-S	5.61	1.25	58.94	0.40	-3.37	1.41	0.01	8.53×10^3	55.31
7-S	5.62	1.18	68.60	0.35	-3.55	2.06	0.01	1.23×10^4	53.56
8-S	5.62	1.12	78.96	0.11	-3.94	22.68	0.01	1.32×10^5	48.07

^aTemperature is 300 K.

11. In ZBPNRs-10, the VBM are composed of s orbitals (proportion is 9.78%), p_z orbitals (proportion is 87.17%), and crossed-ribbon p_y orbitals (proportion is 2.83%); the CBMs are composed of s orbitals (proportion is 16.25%), p_z orbitals (proportion is 63.44%), and p_y orbitals (proportion is 20.31%).

Owing to the unsaturated edges, there are unpaired valence electrons in bare ribbons. Considering the S atom is at the right of the P atom in the periodic table, the case of edge atoms of BPNRs saturated by S atoms is also investigated. We take ABPNR-10 and ZBPNR-7 as examples. The energy band structure of S-terminated BPNRs are very similar to the H-terminated ribbons, as shown in Figure 4. We find that the energy gap of ABPNR-10 with S-termination (1.03 eV) is

almost same as that of H-termination (1.00 eV), but in ZBPNR-7, the gap is smaller (S-termination: 1.21 eV; H-termination: 1.66 eV). The band gap values are shown in Table 1. The mobilities of ABPNR-10 with S-termination are 1.80×10^4 (electron) and 4.06×10^2 (hole) $\text{cm}^2 \text{V}^{-1} \text{s}^{-1}$, which are smaller than those of the H-terminated ABPNRs but higher than those of the bare ABPNRs. The mobilities of ZBPNR-7 with S-termination are 1.12×10^2 (electron) and 1.63×10^3 (hole) $\text{cm}^2 \text{V}^{-1} \text{s}^{-1}$.

With the edge along the \vec{a}_1 (\vec{a}_2) lattice vector in the sheet, the armchair (zigzag) ribbons can be obtained from a BP sheet, like Figure 1a. So when the edges are along \vec{d} ($\vec{d} = \vec{a}_1 + \vec{a}_2$), a diagonal type ribbon is obtained, as shown in Figure 5a. We

denote them as DBPNRs, and the definition of the DBPNR's width (N) is the same as the ABPNRs. For DBPNRs, two types of edge termination are considered: one is bare, and the other is H-terminated. The atomic structure of DBPNRs with H-terminated is similar to the sheet, but there is obvious edge reconstruction in bare DBPNRs. The optimized structure of a bare DBPNR with a width of 6 is shown in Figure 5b. The energy band structures of bare DBPNRs and H-terminated DBPNRs with $N = 6, 7$, and 8 are shown in Figure 5c,d, respectively. Both of the bare and H-terminated DBPNRs are semiconductors, and the H-terminated DBPNR is a Γ point direct gap semiconductor and the energy gap is decreasing with N , which is in good agreement with previous studies;¹⁴ however, the CBM shifts to the Z point in bare DBPNRs.

The lattice length, stiffness, deformation potential constant, and the room-temperature mobility of DBPNRs are shown in Table 2. Because of the edge reconstitution, the bare DBPNRs are stiffer than the H-terminated ribbons. With the increase in the ribbon's width N , we can find the $|E_1|$ of electron is reduced in H-terminated DBPNRs, while it is increased in bare DBPNRs. For both bare and H-terminated DBPNRs, the room-temperature μ_e is much higher than the μ_h . The μ_e of H-terminated DBPNRs is up to $1.70 \times 10^4 \text{ cm}^2 \text{ V}^{-1} \text{ s}^{-1}$ with $N = 8$, which is almost 300 times μ_h , which is only $57.90 \text{ cm}^2 \text{ V}^{-1} \text{ s}^{-1}$. Moreover, there is a smaller difference between the mobilities of electron and hole in bare DBPNRs. With $N = 8$, the μ_e ($162.09 \text{ cm}^2 \text{ V}^{-1} \text{ s}^{-1}$) is about 3 times μ_h ($45.95 \text{ cm}^2 \text{ V}^{-1} \text{ s}^{-1}$) in bare DBPNRs. For H-terminated ribbons, the hole mobilities of DBPNRs are smaller than those of ABPNRs and ZBPNRs. The electron mobilities of DBPNRs are smaller than those of ABPNRs but larger than those of ZBPNRs. Also, we study S-terminated DBPNRs. The energy bands and charge mobilities of S-terminated DBPNRs are shown in Figure S5 and Table 2. It can be found that the electronic structures and charge mobilities of S-terminated DBPNRs are very similar to H-terminated DBPNRs.

In summary, we have calculated the electronic structures and the intrinsic charge carriers mobilities of black phosphorus nanoribbons with the effect of the longitudinal acoustic phonon, using first-principle density functional theory and the Boltzmann transport equation method with the relaxation time approximation. We find that ABPNRs and DBPNRs will transform from indirect gap semiconductors to direct gap semiconductors when edges are passivated, and the energy gap of ZBPNRs can be opened with edge passivated. The numerical results indicate that the maximum μ_e in bare ABPNRs is $3.46 \times 10^3 \text{ cm}^2 \text{ V}^{-1} \text{ s}^{-1}$, which is smaller than that of BP sheet. Furthermore, for the H-terminated ABPNRs, the maximum mobility is up to $1.02 \times 10^7 \text{ cm}^2 \text{ V}^{-1} \text{ s}^{-1}$, which is even higher than graphene. The μ_h in both bare and H-terminated ABPNRs increases continuously with N . The μ_h in bare ABPNRs with $N = 15$ is $\sim 430 \text{ cm}^2 \text{ V}^{-1} \text{ s}^{-1}$ ($576 \text{ cm}^2 \text{ V}^{-1} \text{ s}^{-1}$ for H-termination). The μ_e (μ_h) of H-terminated ZBPNRs increases from 2.80×10^2 (7.72×10^2) to 5.24×10^2 (2.58×10^4) $\text{cm}^2 \text{ V}^{-1} \text{ s}^{-1}$ with $6 \leq N \leq 12$. Unlike the ABPNRs and ZBPNRs, the μ_h in DBPNRs, which is only about $40\text{--}70 \text{ cm}^2 \text{ V}^{-1} \text{ s}^{-1}$, decreases with N . The μ_e in DBPNRs, which increases with N , is higher than μ_h . For $N = 8$, μ_e is up to $1.70 \times 10^4 \text{ cm}^2 \text{ V}^{-1} \text{ s}^{-1}$. Owing to the electron mobility being higher than the hole mobility, ABPNRs and DBPNRs are *n*-type semiconductors, and the mobility difference of the two carriers will be enhanced by the edges terminated by H atoms. Meanwhile, because the hole mobility is about two orders of magnitude larger than the

electron mobility, ZBPNRs has the characteristics of p-type semiconductors in electrical conduction.

ASSOCIATED CONTENT

Supporting Information

The Supporting Information is available free of charge on the ACS Publications website at DOI: [10.1021/acs.jpclett.5b01644](https://doi.org/10.1021/acs.jpclett.5b01644).

Computational details; lattice length, deformation potential, and elasticity modulus of ABPNRs and ZBPNRs. Band structures of S-terminated DBPNRs. (PDF)

AUTHOR INFORMATION

Corresponding Authors

*E-mail: mqlong@csu.edu.cn.

*E-mail: apkschan@cityu.edu.hk.

Notes

The authors declare no competing financial interest.

ACKNOWLEDGMENTS

This work is supported by Hunan Key Laboratory for Supermicrostructure and Ultrafast Process, and the National Natural Science Foundation of China (nos. 61306149 and 11274260), Hong Kong Scholars Program (no. XJ2013003), and the Research Grants Council of Hong Kong SAR (no. cityU 100311/11P).

REFERENCES

- (1) Geim, A. K.; Novoselov, K. S. The rise of graphene. *Nat. Mater.* **2007**, *6*, 183–191.
- (2) Long, M.; Tang, L.; Wang, D.; Li, Y.; Shuai, Z. Electronic Structure and Carrier Mobility in Graphdiyne Sheet and Nanoribbons: Theoretical Predictions. *ACS Nano* **2011**, *5*, 2593–2600.
- (3) Levendorf, M. P.; Kim, C.-J.; Brown, L.; Huang, P. Y.; Havener, R. W.; Muller, D. A.; Park, J. Graphene and boron nitride lateral heterostructures for atomically thin circuitry. *Nature* **2012**, *488*, 627–632.
- (4) Tahir, M.; Schwingenschlogl, U. Valley polarized quantum Hall effect and topological insulator phase transitions in silicene. *Sci. Rep.* **2013**, *3*, 01075.
- (5) Wang, Q. H.; Kalantar-Zadeh, K.; Kis, A.; Coleman, J. N.; Strano, M. S. Electronics and optoelectronics of two-dimensional transition metal dichalcogenides. *Nat. Nanotechnol.* **2012**, *7*, 699–712.
- (6) Xiao, J.; Long, M.-Q.; Li, X.-M.; Zhang, Q.-T.; Xu, H.; Chan, K. S. Effects of Van der Waals interaction and electric field on the electronic structure of bilayer MoS₂. *J. Phys.: Condens. Matter* **2014**, *26*, 405302.
- (7) Cai, Y.; Zhang, G.; Zhang, Y. W. Polarity-Reversed Robust Carrier Mobility in Monolayer MoS₂ Nanoribbons. *J. Am. Chem. Soc.* **2014**, *136*, 6269–6275.
- (8) Li, L.; Yu, Y.; Ye, G. J.; Ge, Q.; Ou, X.; Wu, H.; Feng, D.; Chen, X. H.; Zhang, Y. Black phosphorus field-effect transistors. *Nat. Nanotechnol.* **2014**, *9*, 372–377.
- (9) Liu, H.; Neal, A. T.; Zhu, Z.; Luo, Z.; Xu, X.; Tomanek, D.; Ye, P. D. Phosphorous: An Unexplored 2D Semiconductor with a High Hole Mobility. *ACS Nano* **2014**, *8*, 4033–4041.
- (10) Köpf, M.; Eckstein, N.; Pfister, D.; Grotz, C.; Krüger, I.; Grewe, M.; Hansen, T.; Kohlmann, H.; Nilges, T. Access and in situ growth of phosphorous-precursor black phosphorus. *J. Cryst. Growth* **2014**, *405*, 6–10.
- (11) Lu, W.; Nan, H.; Hong, J.; Chen, Y.; Liang, Z.; Ni, Z.; Jin, C.; Zhang, Z. Plasma-assisted fabrication of monolayer phosphorous and its Raman characterization. *Nano Res.* **2014**, *7*, 853–859.
- (12) Castellanos-Gomez, A.; Vicarelli, L.; Prada, E.; Island, O. J.; Narasimha-Acharya, K. L.; Blanter, S. I.; Groenendijk, D. J.; Buscema,

- M.; Steele, G. A.; Alvarez, J. V.; et al. Isolation and characterization of few-layer black phosphorus. *2D Mater.* **2014**, *1*, 025001.
- (13) Fei, R.; Yang, L. Strain-Engineering the Anisotropic Electrical Conductance of Few-Layer Black Phosphorus. *Nano Lett.* **2014**, *14*, 2884–2889.
- (14) Han, X.; Stewart, H. M.; Shevlin, S. A.; Catlow, C. R. A.; Guo, Z. X. Strain and Orientation Modulated Bandgaps and Effective Masses of Phosphorous Nanoribbons. *Nano Lett.* **2014**, *14*, 4607–4614.
- (15) Wu, M.; Qian, X.; Li, J. Tunable Exciton Funnel Using MoiréSuperlattice in Twisted van der Waals Bilayer. *Nano Lett.* **2014**, *14*, 5350–5357.
- (16) Buscema, M.; Groenendijk, D. J.; Blanter, S. I.; Steele, G. A.; van der Zant, H. S. J.; Castellanos-Gomez, A. Fast and Broadband Photoresponse of Few-Layer Black Phosphorus Field-Effect Transistors. *Nano Lett.* **2014**, *14*, 3347–3352.
- (17) Tran, V.; Soklaski, R.; Liang, Y.; Yang, L. Layer-controlled band gap and anisotropic excitons in few-layer black phosphorus. *Phys. Rev. B: Condens. Matter Mater. Phys.* **2014**, *89*, 235319.
- (18) Tran, V.; Yang, L. Scaling laws for the band gap and optical response of phosphorous nanoribbons. *Phys. Rev. B: Condens. Matter Mater. Phys.* **2014**, *89*, 245407.
- (19) Rodin, A. S.; Carvalho, A.; Castro Neto, A. H. C. Excitons in anisotropic two-dimensional semiconducting crystals. *Phys. Rev. B: Condens. Matter Mater. Phys.* **2014**, *90*, 075429.
- (20) Peng, X.; Wei, Q.; Copple, A. Strain-engineered direct-indirect band gap transition and its mechanism in two-dimensional phosphorous. *Phys. Rev. B: Condens. Matter Mater. Phys.* **2014**, *90*, 085402.
- (21) Lv, H. Y.; Lu, W. J.; Shao, D. F.; Sun, Y. P. Enhanced thermoelectric performance of phosphorous by strain-induced band convergence. *Phys. Rev. B: Condens. Matter Mater. Phys.* **2014**, *90*, 085433.
- (22) Zhu, Z.; Tománek, D. Semiconducting Layered Blue Phosphorus: A Computational Study. *Phys. Rev. Lett.* **2014**, *112*, 176802.
- (23) Guan, J.; Zhu, Z.; Tománek, D. Phase Coexistence and Metal-Insulator Transition in Few-Layer Phosphorous: A Computational Study. *Phys. Rev. Lett.* **2014**, *113*, 046804.
- (24) Guo, H.; Lu, N.; Dai, J.; Wu, X.; Zeng, X. C. Phosphorous Nanoribbons, Phosphorus Nanotubes, and van derWaals Multilayers. *J. Phys. Chem. C* **2014**, *118*, 14051–14059.
- (25) Keyes, R. W. The electrical properties of black phosphorus. *Phys. Rev.* **1953**, *92*, 580–584.
- (26) Warschauer, D. Electrical and optical properties of crystalline black phosphorus. *J. Appl. Phys.* **1963**, *34*, 1853–1860.
- (27) Qiao, J.; Kong, X.; Hu, Z.-X.; Yang, F.; Ji, W. High-mobility transport anisotropy and linear dichroism in few-layer black phosphorus. *Nat. Commun.* **2014**, *5*, 4475.
- (28) Liang, L.; Wang, J.; Lin, W.; Sumpter, B. G.; Meunier, V.; Pan, M. Electronic Bandgap and Edge Reconstruction in Phosphorene Materials. *Nano Lett.* **2014**, *14*, 6400–6406.
- (29) Wang, X.; Jones, A. M.; Seyler, K. L.; Tran, V.; Jia, Y.; Zhao, H.; Wang, H.; Yang, L.; Xu, X.; Xia, F. Highly Anisotropic and Robust Excitions in Monolayer Black Phosphorus. *Nat. Nanotechnol.* **2015**, *10*, 517–521.
- (30) Akahama, Y.; Endo, S.; Narita, S.-I. Electrical properties of black phosphorus single crystals. *J. Phys. Soc. Jpn.* **1983**, *52*, 2148–2155.
- (31) Morita, A. Semiconducting Black Phosphorus. *Appl. Phys. A: Solids Surf.* **1986**, *39*, 227.
- (32) Zhang, J.; Liu, H. J.; Cheng, L.; Wei, J.; Liang, J. H.; Fan, D. D.; Shi, J.; Tang, X. F.; Zhang, Q. J. Phosphorous nanoribbon as a promising candidate for thermoelectric applications. *Sci. Rep.* **2014**, *4*, 6452.
- (33) Wei, Q.; Peng, X. Superior mechanical flexibility of phosphorous and few-layer black phosphorus. *Appl. Phys. Lett.* **2014**, *104*, 251915.
- (34) Liu, H.; Neal, A. T.; Si, M.; Du, Y.; Ye, P. D. The Effect of Dielectric Capping on Few-Layer Phosphorous Transistors: Tuning the Schottky Barrier Heights. *IEEE Electron Device Lett.* **2014**, *35*, 795–797.
- (35) Zhang, S.; Yang, J.; Xu, R.; Wang, F.; Li, W.; Ghafur, M.; Zhang, Y.-W.; Yu, Z.; Zhang, G.; Qin, Q.; Lu, Y. Extraordinary Photoluminescence and Strong Temperature/Angle-Dependent Raman Responses in Few-Layer Phosphorous. *ACS Nano* **2014**, *8*, 9590–9596.
- (36) Deng, Y.; Luo, Z.; Conrad, N. J.; Liu, H.; Gong, Y.; Najmaei, S.; Ajayan, P. M.; Luo, J.; Lou, J.; Xu, X.; Ye, P. D. Black Phosphorous-Monolayer MoS₂ van der Waals Heterojunction p-n Diode. *ACS Nano* **2014**, *8*, 8292–8299.
- (37) Dai, J.; Zeng, X. C. Bilayer Phosphorous: Effect of Stacking Order on Bandgap and Its Potential Applications in Thin-Film Solar Cells. *J. Phys. Chem. Lett.* **2014**, *5*, 1289–1293.
- (38) Kou, L.; Frauenheim, T.; Chen, C. Phosphorous as a Superior Gas Sensor: Selective Adsorption and Distinct I–V Response. *J. Phys. Chem. Lett.* **2014**, *5*, 2675–2681.
- (39) Long, M.-Q.; Tang, L.; Wang, D.; Wang, L.; Shuai, Z. Theoretical Predictions of Size-Dependent Carrier Mobility and Polarity in Graphene. *J. Am. Chem. Soc.* **2009**, *131*, 17728–17729.
- (40) Wang, J.; Zhao, R.; Yang, M.; Liu, Z.; Liu, Z. Inverse relationship between carrier mobility and bandgap in graphene. *J. Chem. Phys.* **2013**, *138*, 084701.
- (41) Kou, L.; Tang, C.; Zhang, Y.; Heine, T.; Chen, C.; Frauenheim, T. Tuning Magnetism and Electronic Phase Transitions by Strain and Electric Field in Zigzag MoS₂ Nanoribbons. *J. Phys. Chem. Lett.* **2012**, *3*, 2934–2941.
- (42) Dolui, K.; Pemmaraju, C. D.; Sanvito, S. Electric Field Effects on Armchair MoS₂ Nanoribbons. *ACS Nano* **2012**, *6*, 4823–4834.
- (43) Xiao, J.; Long, M.; Li, M.; Li, X.; Xu, H.; Chan, K. Carries mobility of MoS₂ nanoribbons with the edge chemical modification. *Phys. Chem. Chem. Phys.* **2015**, *17*, 6865–6873.
- (44) Tang, S.; Zhang, S. Structural and Electronic Properties of Hybrid Fluorographene–Graphene Nanoribbons: Insight from First-Principles Calculations. *J. Phys. Chem. C* **2011**, *115*, 16644–16651.
- (45) Xi, J.; Long, M.; Tang, L.; Wang, D.; Shuai, Z. First-principles prediction of charge mobility in carbon and organic nanomaterials. *Nanoscale* **2012**, *4*, 4348–4369.
- (46) Xiao, J.; Long, M.; Zhang, X.; Ouyang, J.; Xu, H.; Gao, Y. Theoretical predictions on the electronic structure and charge carrier mobility in 2D Phosphorus sheets. *Sci. Rep.* **2015**, *5*, 9961.